Measuring Condensation Heat Transfer on Superhydrophobic Surfaces

Kimberly A. Stevens, Julie Crockett, Daniel Maynes, Brian D. Iverson

April 29, 2019

1 Introduction

Condensation heat transfer is significant in many applications such as such as desalination, energy conversion [1], atmospheric water harvesting [2, 3], electronics cooling, and other high heat flux applications [4]. However, condensate on the surface adds a thermal resistance that limits condensation rates. The rate of condensation heat transfer is inversely proportional to the diameter of the condensate drops[5]. In industrial condensing systems, the resistance is minimized by removing the condensate via gravity or a vapor shear, but the minimum size of droplet removal is typically on the order of the capillary length of the condensate, about 2.7 mm for water.

Properly designed superhydrophobic surfaces have been shown to promote the removal of condensate at drop sizes significantly below the capillary length due to the low contact angle hysteresis (indicating high drop mobility) and coalescence-induced jumping of condensate drops. With the removal of condensate drops due to coalescence-induced jumping, the maximum droplet diameter can be reduced by 1 to 3 orders of magnitude [6, 7]. The potential for superhydrophobic surfaces to significantly impact condensation heat transfer has prompted a great deal of exploratory research regarding the fundamental behavior of condensing droplets on superhydrophobic surfaces. Several works have quantified metrics which indirectly indicate the relative rate of heat transfer on a surface, such as maximum droplet diameter, coarse drop-size distribution, and individual droplet growth rates [8, 9, 10, 11, 12, 13, 14, 15, 16]. Additionally, several models for condensation on superhydrophobic surfaces have been developed [17, 15, 16]. However, only a few works have experimentally measured the heat transfer directly in the absence of NCG [18, 19, 11, 20], and the influence of the micro- and nanostructure geometry on condensation heat transfer is not clear. This work describes preliminary efforts to measure the influence of nano- and microstucture geometry on heat transfer performance.

2 Methods

All experiments were perfomred under vacuum conditions in order to limit the influence of noncondensable gases.

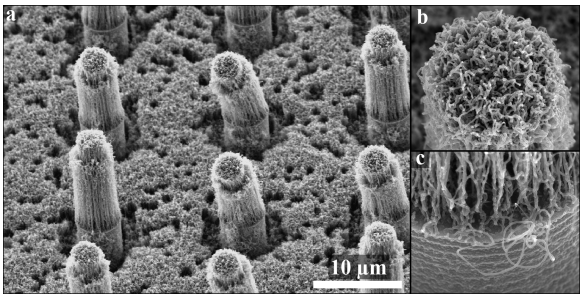

Figure 1: CICNTs grown on top of silicon micropillars. The CICNTs grow on top of the silicon microposts and in the cavities between the posts so that surfaces are covered with the nanostructured CICNTs, creating a two-tiered surface. (b) The top of one of the CICNT clusters (c) The top of the etched silicon post on which a cluster of CICNTs grew.

2.1 Two-Tiered Surfaces

In order to study the influence of a microstructure on condensation heat transfer, two-tiered CICNT surfaces are manufactured. Silicon wafers are etched to create micro ribs or pillars using standard photolithographic procedures [21]. Layers of alumina and iron are deposited and CICNTs are grown uniformly on the surface, both on top of the microscale features and in the cavities between the features. The surfaces are then coated with a layer of PTFE to render them superhydrophobic (but vacuum baking is expected to produce similar results). SEM images of micropillared surfaces are shown in Figure 1. Condensation on the resulting two-tiered surfaces results in coalescence-induced jumping. The surfaces described in previous works, where microfeatures are created by growing CICNTs in a pattern, lacked nanostructures in the space between the features, rendering them ineffective for promoting dropwise condensation.

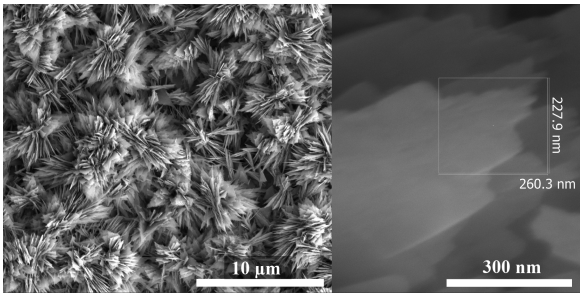

Figure 2: SEM images of the knife-like copper oxide structures.

2.2 Copper Oxide Surfaces

Superhydrophobic copper oxide surfaces are manufactured following the procedures similar to that described in the literature, but with a different functionalization process [22, 23, 24]. Briefly, copper surfaces are polished following the procedure described by Nam and Ju [25], then double-soaked in an ultrasonic acetone bath for 20 minutes, rinsed with ethanol, isopropyl alcohol, and deionized (DI) water 5 times, dried with N_2, and immersed in a 2.0 M solution of HCl for 20 minutes to remove the native oxide film on the surface. The surfaces are then triple-rinsed with DI water and dried with N_2. The nanostructure is created by immersing the substrate in a solution of $NaClO_2$, NaOH, $Na_3PO_4{\cdot}12H_2O$, and DI water (3.75:5:10:100 wt. %) held at 96 ± 3 °C, forming a knife-like copper oxide film as shown in Figure 2. The surface is rinsed 5 times in DI water and dried with N_2. The surface is functionalized by adding two layers of PTFE, applied via spin coating [21]. The resulting surfaces had an advancing contact angle of 157° and hysteresis of 2°. Surfaces are also functionalized using an immersion coating of Glaco [26], which also resulted in superhydrophobic surfaces. Condensation on the copper oxide surfaces resulted in coalescence-induced jumping.

2.3 Heat Flux Measurements

Four independent methods are used to measure the heat flux, motivated by concern that initial heat transfer rates measured on hydrophilic control copper surfaces are lower than that in the literature [5].

- The volume of condensate collected at the bottom of the vacuum chamber is measured. Following a test, the condensate is accessed through the port leading to the Erlenmeyer flask between the needle valve and the chamber with syringe attached to a piece of flexible PVC tubing with a copper wire in the center. The heat transfer rate is calculated from the amount of energy required to condense the amount of liquid collected,

$$q" = \frac{\rho V h_{fg}}{t A_c}, \tag{1}$$

  where t is the length of time of the test, A_c is the condensing area, and V is the volume of collected condensate.

- A heat flux sensor (FluxTeq) is placed between the heat exchanger and copper disk that interfaced with the condensation chamber.

- The temperature gradient in the copper disk interfacing with the chamber is measured. Four thermocouples are embedded in small (#55 drill)

holes. The copper disk is the same size as the condensing surface so that the heat transfer is predominantly one-dimensional. The heat flux through the copper block is calculated as

$$q_{\mathrm{g}}" = -\mathrm{k} A_{\mathrm{c}} \frac{\mathrm{d}T}{\mathrm{d}x}. \quad (2)$$

The temperature gradient is obtained by fitting a line to the temperature measured by the four thermocouples.

- The change in the heat exchanger coolant temperature is measured. Thermocouples measure the water temperature immediately before entering and after exiting the heat exchanger, and a flow meter (Omega FLR1009-D) measures the volumetic coolant flow rate. The heat flux is calculated as

$$q_{\Delta \mathrm{T}}" = \frac{\dot{m} c_p (T_{\mathrm{HXout}} - T_{\mathrm{HXin}})}{A_{\mathrm{c}}}, \quad (3)$$

where T_{HXin} and T_{HXout} is the temperature entering and exiting the heat exchanger.

Agreement between all four methods is generally obtained (within approximately 50%). Uncertainty associated with the condensate collection and heat flux sensor measurements are large so only the heat transfer rate measured from the copper block temperature gradient (q_{g}") and change in coolant temperature ($q_{\Delta \mathrm{T}}$" methods are used for each test. The agreement between these two methods is generally within ±30 % when the heat flux is larger than 10,000 W/m^2, as shown in Figure 3a. However, the measurements rapidly diverged for low heat fluxes. The poor agreement is assumed to stem from the uncertainty associated with the thermocouple position and temperature measurement.

The heat transfer coefficient between the heat exchanger and copper block, U_{HX} is calculated using both approaches and is shown in Figure 3b.

$$U_{\mathrm{HX}} = \frac{q"}{T_{\mathrm{HXin}} - T_{\mathrm{c}}}, \quad (4)$$

The heat transfer coefficient is not expected to change with subcooling. The fact that the heat transfer coefficient changes significantly with subcooling when calculated using the copper block temperature gradient suggests that the change in coolant approach for measuring heat transfer is more accurate at low heat fluxes.

2.4 Saturation Temperature Measurement

Heterogeneous condensation is driven by the temperature difference between the saturated vapor temperature and the surface temperature; it is this temperature difference that is used to calculate a heat transfer coefficient, h, describing the rate of condensation. One reason condensation heat transfer measurements are so challenging is the small temperature difference between the surface and vapor, requiring high precision for accurate results. Experiments are performed with saturation temperatures close to ambient temperature to avoid the need to heat every part of the setup where condensation is undesirable, such as the window through which the condensing surface is observed. However, even with nominally ambient conditions, the vapor temperature is always slightly lower than the surrounding temperature, and a thermocouple placed in the vapor is subject to radiation from the surrounding chamber walls, the cooled condensing surface, and the ring light used to illuminate the surface. A UV filter (Thorlabs FGS600) placed between the ring light and the chamber attenuated the majority of the radiative energy from the light, but error introduced from radiation from other sources is still significant, as evidenced by the disagreement between the saturation pressure measured by the measured vapor pressure and the corresponding saturation temperature measured by the thermocouple. However, after allowing the vapor to equilibrate with the chamber, the agreement between the saturation temperature corresponding to the measured saturation pressure is within 0.05 °C. Accordingly, the saturation temperature is obtained from the measured saturation pressure and the thermocouple in the vapor is used to ensure saturated conditions.

2.5 Surface Temperature Measurement

An original objective of this research is to explore how varying the nano- and microstuctures influenced heat transfer performance. Microstructures are created by etching silicon wafers, while the nanostructures are created by growing CICNTs on Fe coated silion wafers. However, the wafer thickness (∼0.5 mm) precludes thermocouple placement inside the wafer, making it difficult to measure the surface temperature. For high heat fluxes which occur during condensation and low temperature difference between the vapor and surface, even small contact resistance between the copper block and the wafer is significant. Additionally, since most thermal greases and pastes have vapor pressures higher than 3 Pa, they could not be used to minimize the contact resistance, necessitating the use of vacuum grease as a substitute thermal interface material.

It is also difficult to accurately quantify the contact resistance. The condensing surface temperature could not be measured using an IR camera during condensation since the condensate obscured the view of the surface. Surface temperature measured by a thermocouple adhered to the condensing surface is also affected by the temperature of the condensate and introduced another contact resistance between the surface and thermocouple. If the contact resistance were measured by heating one side of the interface and cooling the other with forced convection, the chamber would be required to be at atmospheric pressure; in this case, the contact resistance may not behave the same when the junction is exposed to ambient temperature saturation pressure (approximately 2.7 kPa). CICNTs can be grown on stainless steel surfaces, and a thermocouple could be embedded in a stainless steel surface. This was attempted, but the uncertainty introduced by the size of a hole (#55 drill) for the thermocouple is unviably large, since the thermal conductivity of stainless steel is small relative to copper. Accordingly, superhydrophobic copper oxide surfaces are manufactured which allow surface temperature measurement by placing a thermocouple in a hole drilled through the side. Unfortunately, a method to control the micro- and nanostructure of copper oxide surfaces was not obtained.

2.6 Use of Computer Vision

Minimizing the uncertainty associated with traditional heat flux measurement methods (heat flux sensors, thermocouple arrays, change in coolant temperature, condensate collection etc.) to an acceptably low level can be challenging, and generally provide little to no spatial information and may have significant time delays. In contrast, optical microscopes provide extremely detailed spatial information with relatively little time delay. Accordingly, computer vision analysis of optical microscope videos to obtain heat transfer measurements offers a promising alternative and was successfully used by Ölçeroğlu *et al.* [12]. A MATLAB code was written, capable of autonomously tracking thousands of individual drops. The code successfully tracks drops when the nucleation density is extremely low and the space between drops is large, as occurs during condensation in ambient conditions with large concentrations of NCG. The computer vision code estimated the heat transfer rate during condensation on a two-tiered superhydrophobic surface experiencing coalescence-induced jumping by tracking the size of all departing drops [27]. During steady state condensation, the rate of condensate production can be estimated from the rate of condensate departure, and the heat transfer rate is calculated using Equation 1. The code used a combination of the contrast in intensity between drops and surroundings and the Hough transform to distinguish the drops. On the first frame of the video, the location and radius of each of the drops of condensate is detected. The code then tracks the growth of each droplet in the first frame through time until the drop coalesces with a neighboring drop or the video ends. Additional drops that nucleate in subsequent frames are detected and similarly tracked through time. This approach for measuring condensation heat transfer works well in the presence of NCG, but heat transfer measurements obtained in the presence on NCG are not useful for comparison across experimental setups since the heat transfer rate is limited by the vapor diffusion rate to the surface.

In the absence of NCG and with a reasonable de-

gree of subcooling, the nucleation density is so high that a significant number of small drops are hidden in the shadow of large drops when the contact angle is high, rendering the task of tracking every drop impossible. However, on a surface where all drops eventually depart via coalescence-induced jumping, if it were possible to track every departure event one could still obtain an estimate of the heat transfer rate; this could be accomplished by measuring the condensate departure rate, equivalent to the condensate production rate during steady state condensation. Unfortunately, the high nucleation density renders the task of tracking every departure difficult. The code uses the contrast between the substrate and drops to track individual drops; when drops cover every part of the condensing surface they are difficult to distinguish. Due to these challenge of measuring drop departure with high nucleation density, computer vision was not used to obtain heat transfer measurements. However, for condensation in the presence of non-condensable gases the nucleation density is so much lower than this approach is a viable approach for heat transfer measurement, as demonstrated by Olceroglu et al. [12]

3 Preliminary Results

The heat flux measured during condensation on nanostructured CICNT surfaces using the change in coolant temperature is shown in Figure 4. The heat transfer rate increases with increasing subcooling, as expected. The overall heat transfer coefficient, U, is calculated from the measured heat transfer rate and the difference between the vapor temperature and the surface temperature (represented by the thermocouple closest to the surface of copper block). Therefore, the overall heat transfer coefficient includes the condensation heat transfer coefficient and the following thermal resistances: (1) the CICNT nanostructure, (2) Fe and alumina coated-silicon wafer, (3) copper between the thermocouple placement and the surface, and (4) the contact resistance. However, of these thermal resistances, all are estimated to have a negligible impact on U except the contact resistance. The experimentally observed overall heat transfer coefficient generally decreases with increasing subcooling. Since the contact resistance should remain constant with increased subcooling, the decrease in overall heat transfer coefficient indicates that the condensation heat transfer coefficient is decreasing, as observed by other investigators [20, 11, 19], but in contrast to that predicted by classic dropwise condensation heat transfer predictions [5].

The change in vacuum chamber pressure is measured after allowing the chamber to pump down for at least 24 hours, but before introducing water vapor. However, the longer the chamber is under vacuum, the lower the rate of pressure rise, indicating that the increase in pressure is likely due to outgassing. The influence of the initial rate of pressure rise on heat transfer performance is shown in Figures 4a and b. Despite careful efforts to minimize the influence of NCG, it appears that performance may be slightly decreased when initial rate of pressure rise is greater than 0.15 Pa/min. The concentration of NCG is conservatively estimated by multiplying the outgassing rate by length of time since the introductino of water vapor, and adding it to the initial vacuum pressure (3 Pa) and dividing by the water vapor pressure ($\sim$2.7 kPa). The estimate is conservative because the pressure rise is non-linear and the rate of pressure rise decreases over time. Furthermore, it is expected that the introduction of water vapor would significantly reduce the rate of pressure rise. For an hour long test with an initial rate of pressure rise 0.15 Pa/min, the NCG concentration would be 0.4%, less than the standard of 0.6% met by all test presented. Therefore, it is recommended that future tests be conducted with a lower NCG concentration standard than 0.6%. Ideally, the NCG concentration would be less than 0.25%, as described in the Supporting Information of Miljkovic *et al.* [18].

The length of time since condensation commencement on the heat transfer rate (Figure 4c and d) appears to have little influence. The condensation rate appears slightly higher with increased condensation time, contrary to what might be expected if the NCG concentration were increasing with time. The apparent increase in heat transfer performance with time may be a result of larger drops on the surface, or more water within the nanostructure, leading to a

higher percentage of partially wetting drops, which are expected to have a higher heat transfer rate than suspended drops [15].

The CICNT diameter ranged from 25 to 125 nm; surfaces with CICNT diameter larger than 60 nm appeared to have diminished heat transfer performance relative to those with smaller diameters. However, given the fact that these surfaces all flooded the decrease in performance is expected.

4 Conclusions and Future Work

Heat transfer measurements on plain CICNT surfaces are obtained, with diminished heat transfer performance for surfaces which experienced flooding. The heat transfer measurements included the contact resistance between the surface and cooled copper block, confounding isolatio of the condensation heat transfer coefficient. A process for manufacturing copper oxide superhydrophobic surfaces, which allows the measurement of the surface temperature, is described. However, heat transfer measurements have not yet been obtained on these surfaces. Since the copper oxide surfaces do not offer control over the micro- and nanostructure, the objective of exploring micro- and nanostructured surfaces cannot be realized. However, heat transfer measurements could be compared with the drop behavior statistics obtained from video/computer vision analysis (drop-size distribution, drop-departure-size distribution, percent of coalescence events resulting in departure, maximum drop size, etc.). A process for manufacturing two-tiered superhydrophobic surfaces is described offering control of the nanostructure and microstructure. Since the surface is created using Si wafers, measurement of the surface temperature is not possible; however, comparative heat transfer measurements (as in this the present work), could be obtained, providing information regarding the relative influence of two-tiered geometry (e.g. microstructure height, pitch, and shape; nanostructure diameter and height) on heat transfer performance.

References

[1] L. R. Glicksman and A. W. Hunt, "Numerical simulation of dropwise condensation," *International Journal of Heat and Mass Transfer*, vol. 15, no. 11, pp. 2251–2269, 1972.

[2] J. C. Love, L. A. Estroff, J. K. Kriebel, R. G. Nuzzo, and G. M. Whitesides, "Self-assembled monolayers of thiolates on metals as a form of nanotechnology," *Chemical Reviews*, vol. 105, no. 4, pp. 1103–1169, 2005.

[3] H. G. Andrews, E. A. Eccles, W. C. Schofield, and J. P. Badyal, "Three-dimensional hierarchical structures for fog harvesting," *Langmuir*, vol. 27, no. 7, pp. 3798–3802, 2011.

[4] R. N. Leach, F. Stevens, S. C. Langford, and J. T. Dickinson, "Dropwise condensation: experiments and simulations of nucleation and growth of water drops in a cooling system," *Langmuir*, vol. 22, no. 21, pp. 8864–8872, 2006.

[5] J. W. Rose, "Dropwise condensation theory and experiment: A review," *Proceedings of the Institution of Mechanical Engineers Part A: Journal of Power and Energy*, vol. 216, no. A2, pp. 115–128, 2002.

[6] J. B. Boreyko and C.-H. Chen, "Self-propelled dropwise condensate on superhydrophobic surfaces," *Physical Review Letters*, vol. 103, no. 18, p. 184501, 2009.

[7] H. Cha, C. Xu, J. Sotelo, J. M. Chun, Y. Yokoyama, R. Enright, and N. Miljkovic, "Coalescence-induced nanodroplet jumping," *Physical Review Fluids*, vol. 1, no. 6, p. 064102, 2016.

[8] X. Chen, J. Wu, R. Ma, M. Hua, N. Koratkar, S. Yao, and Z. Wang, "Nanograssed micropyramidal architectures for continuous dropwise condensation," *Advanced Functional Materials*, vol. 21, no. 24, pp. 4617–4623, 2011.

[9] K. Rykaczewski, A. T. Paxson, S. Anand, X. Chen, Z. Wang, and K. K. Varanasi, "Multimode multidrop serial coalescence effects during condensation on hierarchical superhydrophobic surfaces," *Langmuir*, vol. 29, no. 3, pp. 881–891, 2013.

[10] P. Zhang, Y. Maeda, F. Lv, Y. Takata, and D. Orejon, "Enhanced coalescence-induced droplet-jumping on nanostructured superhydrophobic surfaces in the absence of microstructures," *ACS Applied Materials and Interfaces*, vol. 9, no. 40, pp. 35 391–35 403, 2017.

[11] R. Wen, S. Xu, D. Zhao, Y.-C. Lee, X. Ma, and R. Yang, "Hierarchical superhydrophobic surfaces with micropatterned nanowire arrays for high-efficiency jumping droplet condensation," *ACS Applied Materials and Interfaces*, vol. 9, no. 51, pp. 44 911–44 921, 2017.

[12] E. Ölçeroğlu, C.-Y. Hsieh, M. M. Rahman, K. K. S. Lau, and M. McCarthy, "Full-field dynamic characterization of superhydrophobic condensation on biotemplated nanostructured surfaces," *Langmuir*, vol. 30, no. 25, pp. 7556–7566, 2014.

[13] C. S. Sharma, J. Combe, M. Giger, T. Emmerich, and D. Poulikakos, "Growth rates and spontaneous navigation of condensate droplets through randomly structured textures," *ACS Nano*, 2017.

[14] A. Aili, Q. Ge, and T. Zhang, "How nanostructures affect water droplet nucleation on superhydrophobic surfaces," *Journal of Heat Transfer*, vol. 139, no. 11, pp. 112 401–112 401–10, 2017.

[15] N. Miljkovic, R. Enright, and E. N. Wang, "Effect of droplet morphology on growth dynamics and heat transfer during condensation on superhydrophobic nanostructured surfaces," *ACS Nano*, vol. 6, no. 2, pp. 1776–1785, 2012.

[16] S. Chavan, H. Cha, D. Orejon, K. Nawaz, N. Singla, Y. F. Yeung, D. Park, D. H. Kang, Y. Chang, Y. Takata, and N. Miljkovic, "Heat transfer through a condensate droplet on hydrophobic and nanostructured superhydrophobic surfaces," *Langmuir*, vol. 32, no. 31, pp. 7774–7787, 2016.

[17] S. Kim and K. J. Kim, "Dropwise condensation modeling suitable for superhydrophobic surfaces," *Journal of Heat Transfer*, vol. 133, no. 8, p. 081502, 2011.

[18] N. Miljkovic, R. Enright, Y. Nam, K. Lopez, N. Dou, J. Sack, and E. N. Wang, "Jumping-droplet-enhanced condensation on scalable superhydrophobic nanostructured surfaces," *Nano Letters*, vol. 13, no. 1, pp. 179–187, 2013.

[19] R. Wen, Q. Li, J. Wu, G. Wu, W. Wang, Y. Chen, X. Ma, D. Zhao, and R. Yang, "Hydrophobic copper nanowires for enhancing condensation heat transfer," *Nano Energy*, vol. 33, pp. 177–183, 2017.

[20] R. Wen, S. Xu, X. Ma, Y.-C. Lee, and R. Yang, "Three-dimensional superhydrophobic nanowire networks for enhancing condensation heat transfer," *Joule*, vol. 2, no. 2, pp. 269–279, 2018.

[21] J. Prince, "The influence of superhydrophobicity on laminar jet impingement and turbulent flow in a channel with walls exhibiting riblets," Thesis, Brigham Young University, 2013.

[22] R. Enright, N. Miljkovic, N. Dou, Y. Nam, and E. N. Wang, "Condensation on superhydrophobic copper oxide nanostructures," *Journal of Heat Transfer*, vol. 135, no. 9, p. 091304, 2013.

[23] N. Miljkovic and E. N. Wang, "Condensation heat transfer on superhydrophobic surfaces," *MRS Bulletin*, vol. 38, pp. 397–406, 2013.

[24] H. Cha, J. M. Chun, J. Sotelo, and N. Miljkovic, "Focal plane shift imaging for the analysis of dynamic wetting processes," *ACS Nano*, vol. 10, no. 9, pp. 8223–8232, 2016.

[25] Y. Nam and Y. S. Ju, "A comparative study of the morphology and wetting characteristics of micro/nanostructured cu surfaces for

phase change heat transfer applications," *Journal of Adhesion Science and Technology*, vol. 27, no. 20, pp. 2163–2176, 2013.

[26] G. Dupeux, P. Bourrianne, Q. Magdelaine, C. Clanet, and D. Qur, "Propulsion on a superhydrophobic ratchet," *Scientific Reports*, vol. 4, pp. 5280–5280, 2014.

[27] K. A. Stevens, J. Crockett, D. R. Maynes, and B. D. Iverson, "An optical-based aggregate approach to measuring condensation heat transfer," in *Utah Space Grant Consortium Proceedings*, 2017, Conference Proceedings. [Online]. Available: https://digitalcommons.usu.edu/spacegrant/2017/S

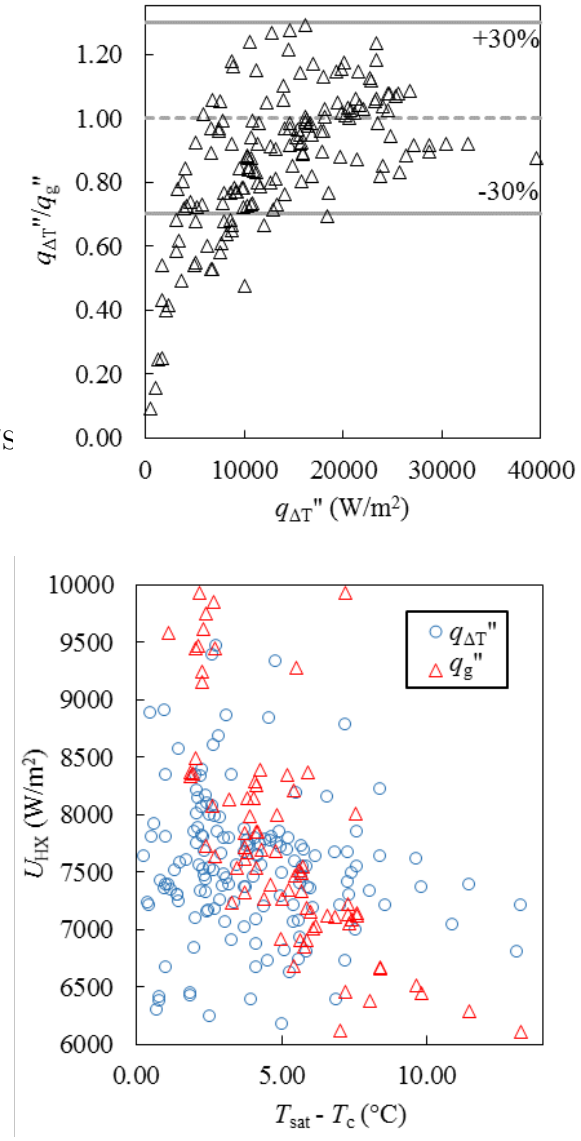

Figure 3: (a) Ratio between heat transfer measurements made using the change in coolant temperature and the temperature gradient in the copper block. (b) Heat transfer coefficient between the heat exchanger and copper block obtained using the change in coolant temperature and copper block temperature gradient approaches for measuring the heat transfer rate.

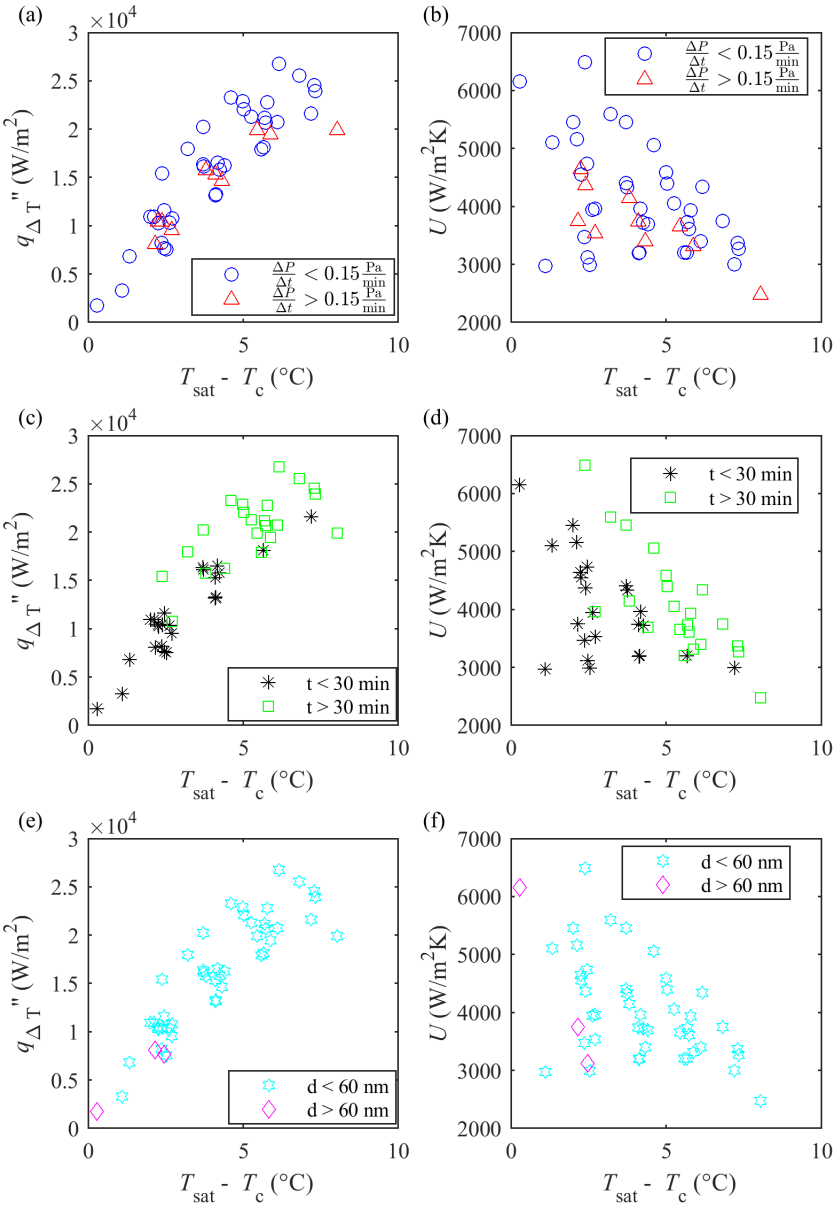

Figure 4: (a,c,e) Condensation heat flux, q", measured using the change in heat exchanger coolant temperature on CICNT coated surfaces and (b,d,f) the total heat transfer coefficient, U as a function of subcooling temperature. This overall heat transfer coefficient includes the condensation heat transfer coefficient and contact resistance. The markers in (a,b) indicate tests where the rate of pressure rise (likely due to outgassing) is less than 0.15 Pa/min (blue circles) or greater than 0.15 Pa/min (red triangles). The markers in (c,d) indicate data taken less than (blue circles) or more than (red triangles) 30 minutes since the beginning of condensation. The markers in (e,f) indicate surfaces with CICNT diameter less than (blue circles) or greater than (red triangles) 60 nm.